Journal of the Meteorological Society of Japan, Vol. 90, No. 2, pp. 179–190, 2012
DOI:10.2151/jmsj.2012-202

A Spatial-Temporal Projection Method for Seasonal Prediction of Spring Rainfall in Northern Taiwan

Pang-chi HSU, Tim LI

International Pacific Research Center, University of Hawaii, Honolulu, Hawaii, USA

Yun-Ching LIN, Mong-Ming LU

Central Weather Bureau, Taipei, Taiwan

and

June-Yi LEE

International Pacific Research Center, University of Hawaii, Honolulu, Hawaii, USA

(Manuscript received 9 December 2010, in final form 22 November 2011)

Abstract

A spatial-temporal projection method (STPM) is developed to predict the spring (March–May, MAM) rainfall in northern Taiwan. Seven large-scale atmospheric and oceanic fields (925-hPa zonal wind, meridional wind, and moisture, 850-hPa, 500-hPa, and 200-hPa geopotential height, and sea surface temperature) with their temporal evolutions during the preceding 11 months are used as predictors. An optimal ensemble (OE) strategy is developed based on the best cross-validation results from each predictor over the training period. Some predictors adopted in the OE show the longest lead time of 10-month. The deterministic forecast result based on the OE approach indicates that the STPM predictions are skillful with an averaged temporal correlation coefficient of 0.6. However, the amplitude of the forecasted rainfall is underestimated, which is treated by introducing an amplifier coefficient. The STPM is also skillful for the probabilistic prediction of spring rainfall in northern Taiwan. The averaged Brier skill score reaches 0.37 for the below-normal categorical case.

1. Introduction

Seasonal rainfall evolutions in Taiwan are closely related to the East Asian monsoon (Tao and Chen 1987; Yen and Chen 2000; Chen and Chen 2003). During the southwesterly summer monsoon, the wet Mei-yu season occurs in mid-May to June followed by the main tropical cyclone season from June to August. The driest period occurs during the northeasterly winter monsoon. During the spring transition, rainfall amount poses a serious challenge for water resource management since deficient spring rainfall can lead to an extension of the dry winter period. Thus, an accurate prediction of spring rainfall is critical for Taiwan.

The rainfall pattern in spring (March to May, MAM) reveals a significantly geographical feature over the is-

Corresponding author: Tim Li, IPRC, SOEST, University of Hawaii at Manoa, 1680 East West Road, POST Bldg. 401, Honolulu, HI 96822, USA.
E-mail: timli@hawaii.edu

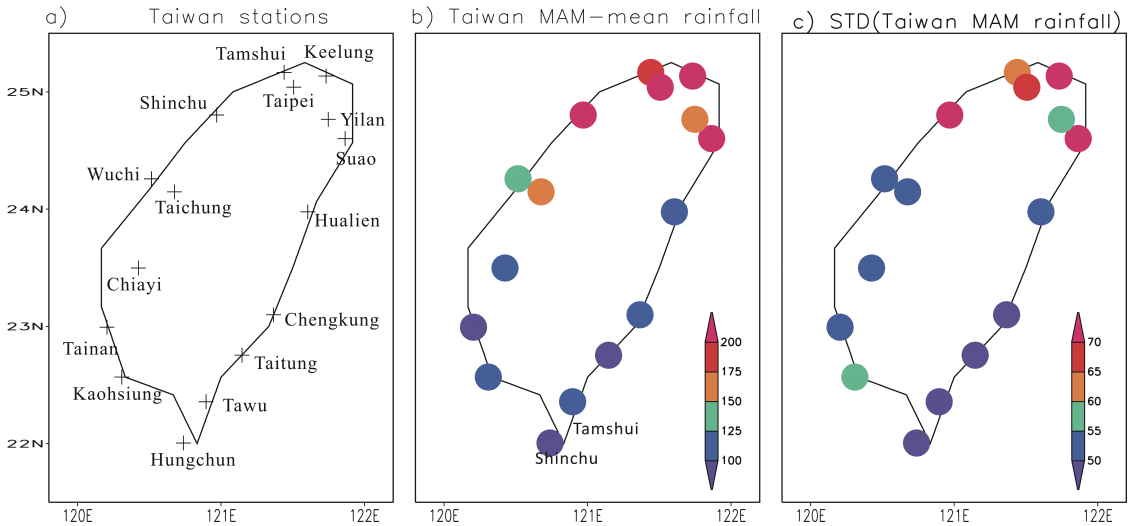

Fig. 1. (a) Locations of major rainfall stations in Taiwan. (b) Mean and (c) Standard deviation of March–May rainfall (mm) during the period of 1979–2009.

land of Taiwan (Fig. 1). The MAM rainfall is relatively large in northern Taiwan, while it is much less in southern Taiwan (e.g., Hung et al. 2004). The averaged rainfall rates in MAM are greater than 150 mm in most stations north of 24.5°N (Fig. 1b). The standard deviations in anomalous MAM rainfall at these stations are large as well, indicating that the interannual variability of the spring rainfall is vigorous in northern Taiwan (Fig. 1c).

A number of investigators have studied the factors that may affect the spatial and temporal variations of spring rainfall in Taiwan (e.g., Chen et al. 2003; Jiang et al. 2003; Chen and Chen 2003; Hung et al. 2004; Chen et al. 2008), particularly the relationship between El Niño-Sothern Oscillation (ENSO) and spring rainfall in Taiwan. In general, enhanced Taiwan spring rainfall occurs when an El Niño condition occurs in the equatorial eastern Pacific in the preceding winter (Chen et al. 2003). Jiang et al. (2003) used correlation analysis from 1951–2000 to show that the February–March rainfall in Taiwan is significantly correlated with the Niño3 sea surface temperature (SST) anomaly (SSTA) from the preceding November to March. The anomalous Philippine Sea anticyclone (PSAC, Chang et al. 2000; Wang et al. 2001; Wu et al. 2009) formed during the El Niño developing and mature phases (Wu et al. 2010) plays a role in inducing anomalous southwesterly flows that transport surface moisture from the South China Sea to the vicinity of Taiwan. This moisture transport favors intensified rainfall activity during spring (Chen et al. 2003; Jiang et al. 2003). In addition, the ENSO-induced mid-latitude frontal system (Wang and Zhang 2002; Chen et al. 2003) and variability of the Pacific subtropical high (Lu 2001; Chen et al. 2008) may also modulate the interannual variability of spring rainfall in Taiwan.

The positive correlation between ENSO and spring rainfall in Taiwan, however, is not always observed. Chen et al. (2008) found that Taiwan's spring rainfall may be either increased or decreased by an El Niño (or a La Niña) event. This asymmetric relationship between spring rainfall and ENSO is partially attributed to the effect of the SSTA in the tropical Indian Ocean and associated anomalous large-scale circulations. The significant spring rainfall in Taiwan occurs only when both an El Niño and a positive SSTA in the tropical Indian Ocean co-exist. Under the condition of the combined eastern Pacific and Indian Ocean warm SSTA forcing, a subsidence appears in the Philippine Sea and maintains the PSAC (e.g., Watanabe and Jin 2002). This result manifests the role of the Indian Ocean SSTA in the Taiwan spring rainfall. Hung et al. (2004) found that spring rainfall fluctuations in northern Taiwan are closely related to the Pacific Decadal Oscillation (PDO), which is characterized by SST oscillations in the mid-latitude North Pacific.

Besides the remote and local SSTA forcing, the spring rainfall in Taiwan is affected by synoptic systems, such as frontal trough and low- and high-level jets (Chen et al. 2003; Chen and Chen 2003). Wu and Kirtman (2007) indicated that the winter and spring

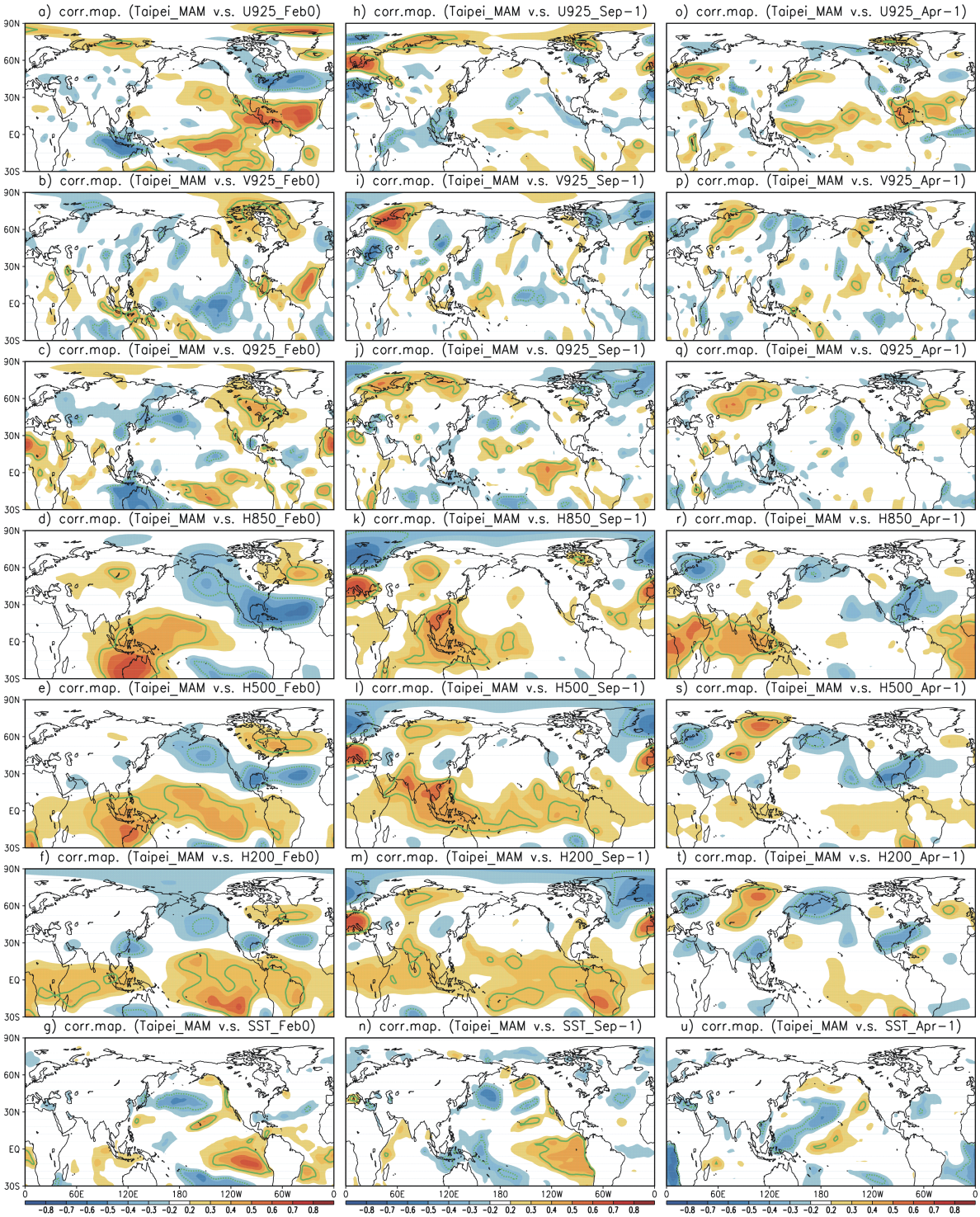

Fig. 2. Correlation coefficients (shaded) between March–May rainfall in Taipei and seven large-scale predictors (from top to bottom: U925, V925, Q925, H850, H500, H200 and SST) in preceding February (left panel), September (central panel) and April (right panel) for the period of 1979–2009. The green contour indicates that the correlation exceeds a 95% confidence level.

snow covers over Eurasia are significantly related to the spring rainfall in East Asia. Their results suggested that the land surface forcing may also play a role in modulating the spring rainfall in Taiwan. Moreover, the North Atlantic Oscillation (NAO) and Arctic Oscillation (AO) could affect the East Asian climate in northern spring (Gong and Ho 2003; Yang et al. 2004).

Figure 2 shows lagged correlation maps between MAM rainfall in Taipei and various large-scale atmospheric and oceanic fields at a lead of 1 month, 6 months, and 11 months respectively. For different time lags, the significant (with a 95% confidence level or above) correlations between the spring rainfall and the large-scale fields appear in various regions. For instance, a notable positive SSTA is observed in the equatorial eastern Pacific at one month lead in February (Fig. 2g), while an anticyclonic circulation occurs at 850 hPa and 500 hPa in the northwestern Australian and tropical western North Pacific regions (Figs. 2d, e). The low-level anticyclonic circulation may generate enhanced southwesterly flows that transport moisture to Taiwan and enhance the spring rainfall there (Chen et al. 2003). At the same lead, the Taipei rainfall shows a significant correlation with the geopotential height fields over the Atlantic Ocean (Figs. 2d, e), suggesting that the MAM rainfall in Taipei might be remotely related to the NAO from the preceding February.

At a 6-month lead, the SST warming over the eastern Pacific becomes weaker, while a significant negative SSTA appears in the tropical western Pacific (Fig. 2n). The prominent associations of the geopotential height fields with the MAM rainfall occur in the South Asia and maritime continents. The geopotential height features become less clear over the Atlantic in the preceding September (Figs. 2k, l).

At the 11-month lead, a significant cold SSTA appears in the Philippine Sea, while a warm SSTA is found in the central Pacific extending northeastward (Fig. 2u). An enhanced high pressure at 850 hPa appears in the Indian Ocean, northern Africa and southern Atlantic (Fig. 2r). In the middle and upper troposphere, the Siberian high and Aleutian low are strengthened (Figs. 2s, t). The wind and moisture fields also exhibit significant correlations in some regions at such a long lead.

The results above suggest that spring rainfall in Taiwan is, to a large extent, modulated by large-scale atmospheric and oceanic conditions in different regions. A conventional regression model using either an area averaged field or a spatially varying large-scale field at a zero lead as a predictor may have difficulties in generating a skillful spring rainfall forecast. Considering both the spatial and temporal linkages between Taiwan spring rainfall and large-scale fields, we developed a statistical model referred to as a spatial-temporal projection method (STPM) in this study. The data and the methodology are described in Section 2. The deterministic and probabilistic forecast results of spring rainfall for the period of 1979–2009 are given in Section 3. Section 4 presents a summary.

2. Data and methodology

2.1 Data

Spring rainfall data in Taiwan are from the Taiwan Central Weather Bureau (CWB). As shown in Fig. 1, stations north of 24.5°N reveal a large rainfall rate and a prominent interannual variability. Because the rainfall record in Suao is relatively short, the MAM rainfall anomalies in 5 major stations in northern Taiwan (i.e., Taipei, Tamshui, Keelung, Hsinchu and Yilan) are selected as predictands.

The following seven large-scale dynamic and thermodynamic variables are selected as predictors. They are zonal and meridional wind fields at 925 hPa (U925, V925), specific humidity at 925 hPa (Q925), geopotential height at 850, 500 and 200 hPa (H850, H500, H200), and SST.

Two monthly datasets are utilized. The global SST field is obtained from the National Oceanic and Atmospheric Administration/National Climatic Data Center (NOAA/NCDC) Extended Reconstructed Sea-Surface Temperature version 2 (ERSST V2) dataset (Smith and Reynolds 2004) with a $2^\circ \times 2^\circ$ resolution. Other atmospheric variables are obtained from the National Centers for Environmental Prediction-National Center for Atmospheric Research (NCEP-NCAR) global atmospheric reanalysis dataset (Kalnay et al. 1996) at a $2.5^\circ \times 2.5^\circ$ grid. Both the datasets above cover a period from 1950 to the present. In this study we only use a period of 1979–2009 for the spring rainfall forecast study because the relationship between the spring rainfall in Taiwan and atmospheric circulation/SST anomalies is subject to an interdecadal variability, and the most significant correlation is found since the late 1970s when a climate regime shift associated with the PDO occurs (Jiang et al. 2003).

2.2 A Spatial-Temporal Projection Method (STPM)

The key feature of the STPM is that we consider not only spatially varying large-scale fields in the month prior to the forecast time, but also the temporal evolution of the large-scale patterns in the preceding 11 months. This method is an extension of Kug et al. (2007), who used regional SSTA patterns (e.g., in Niño

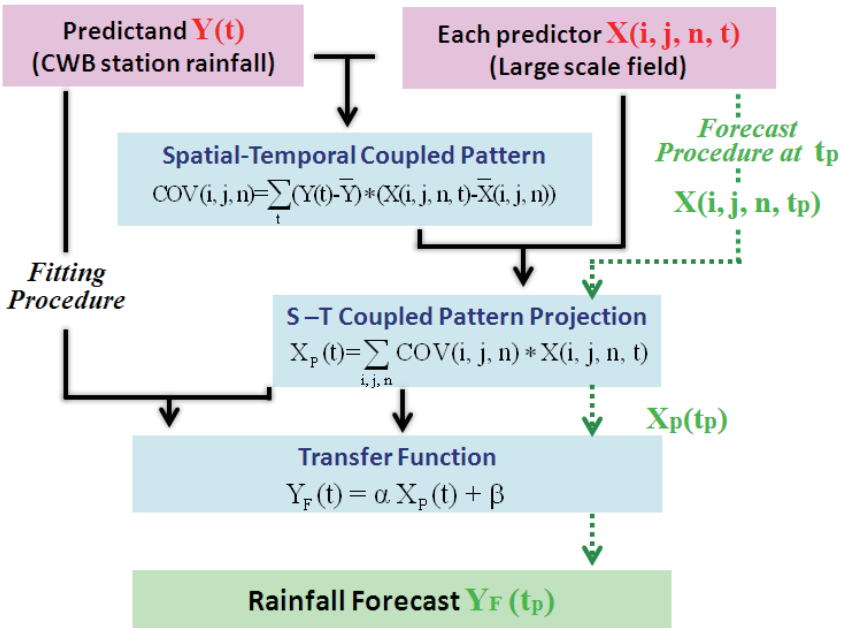

Fig. 3. The major steps of STPM forecast. X and Y are predictor and predictand respectively. An overbar represents the time mean over a training period. i, j denote spatial grids, n indicates preceding nth month prior to forecast month, and t is temporal grid. Other functions and coefficients may refer to Subsection 2.2. Solid black arrows indicate the developing procedures of STPM forecast model. Forecast procedures are denoted by green dashed arrows.

3 region) and historical SSTA fields in the past months to predict the global SSTA field.

To take into account the temporally evolving correlation patterns for each of the seven predictors, we only calculate the coupled pattern projection coefficient in the regions where the covariance pattern between the spring rainfall anomaly and the antecedent large-scale dynamic and thermodynamic predictor fields exceed the 95% significance level. The detailed procedures of the STPM are described as followed (see also Fig. 3).

1) Construct spatial-temporal coupled co-variance patterns (COV) for the region where predictand Y and predictor field X are significantly correlated (>95% significant level).

$$COV(i,j,n) = \sum_t (Y(t) - \overline{Y}) * (X(i,j,n,t) - \overline{X}(i,j,n))$$

where i, j denote spatial grids, n indicates preceding nth month prior to forecast month, and t is temporal grid, respectively. The forecast skills of a temporally evolving predictor field versus an individual month predictor will be compared in Section 3. An overbar represents the time mean over a training period. One may omit $\overline{Y}$ and $\overline{X}$ if the input Y and X have been normalized based on their standard deviations after the climatological annual cycle fields are removed.

2) The coupled pattern projection coefficient is obtained by multiplying the co-variance field and each predictor and sum the product for each grid point (at each lag) where a 95% significant level is reached.

$$X_p(t) = \sum_{i,j,n} COV(i,j,n) * X(i,j,n,t)$$

3) The transfer function is constructed with a linear regression method. The parameters α and β are the regression coefficients of the projected time series, X_p, on the predictand during a training period.

$$Y_F(t) = \alpha X_p(t) + \beta$$

4) The rainfall forecast at time t_p is performed based on the coupled pattern projection and transfer function.

$$X_p(t_p) = \sum_{i,j,n} COV(i,j,n) * X(i,j,n,t_p)$$
$$Y_F(t_p) = \alpha X_p(t_p) + \beta$$

2.3 *Optimal ensemble*

An optimal ensemble forecast strategy is developed by omitting the poor models that may degrade fore-

cast skills. To examine the practical skill of the optimal ensemble forecast, both the double cross-validation method (Feddersen et al. 1999; Kug et al. 2008) and an independent forecast via a moving training window (Kug et al. 2007) are used in this study. During a training period, the prediction target is particularly excluded. The MAM rainfall hindcast is made by each of seven predictor with a different lead-month (i.e., FJDNOSAJJMA, JDNOSAJJMA, DNOSAJJMA, ⋯, MA, A) based on the STPM mentioned above. For each predictor with different preceding months, the prediction with the highest temporal correlation coefficient (TCC) between observed and STMP-predicted MAM rainfall during the training period is selected for the optimal ensemble forecast. A simple arithmetic average is then applied to these seven optimal model predictions to obtain the final deterministic prediction. On the other hand, the selected optimal predictions could be treated as seven ensemble members for probabilistic forecast. Hereafter, this optimal ensemble method is referred to as OE.

To obtain the best forecast skill, we further select the most skillful predictions whose TCC scores exceed a 90% significance level for optimal ensemble. This optimal ensemble based on the 90% significance level is referred to as OE_sig. Note that the significance threshold may change with the length of the training period. For a 30-year training period (i.e., 30 independent, normally distributed samples), the 90% significance level corresponds to a TCC of 0.3. To examine whether the OE approach improves spring rainfall forecast skill, a simple composite of all 77 prediction models (7 large-scale predictors, each of which has 11 different lead-month cases) is also performed and is named as the simple ensemble (SE). As seen from the subsequent results, the OE_sig/OE predictions are, in general, better than the SE because the formers exclude models with low skills.

2.4 *Forecast quality evaluation*

The metrics used to evaluate the deterministic prediction skill of STMP include the TCC and the root-mean-square error (RMSE). The probabilistic forecast skill is measured by the Brier Skill Score (BSS), which is similar to the RMSE used for assessing the deterministic prediction skill. Following Wilks (1995), a Brier score (BS) is defined as

$$\mathrm{BS} = \frac{1}{n}\sum_{i=1}^{n}(f_i - o_i)^2$$

where i refers to the forecast-observation pairs and n is the total number of such pairs, f_i is the forecast probability of occurrence for the ith forecast, and o_i is the ith observed probability (0 if it doesn't happen and 1 if it happens). The BS can be decomposed as three terms: reliability, resolution and uncertainty as follows (Murphy 1973; Wilks 1995):

$$\begin{aligned}\mathrm{BS} &= \underbrace{\frac{1}{n}\sum_{k=1}^{m} n_k(f_k - \overline{o}_k)^2}_{\text{reliability}} - \underbrace{\frac{1}{n}\sum_{k=1}^{m} n_k(\overline{o}_k - \overline{o})^2}_{\text{resolution}} + \underbrace{\overline{o}(1-\overline{o})}_{\text{uncertainty}} \\ &= b_{\mathrm{rel}} - b_{\mathrm{res}} - b_{\mathrm{unc}}\end{aligned}$$

where n is the total number of forecasts issued, m indicates the number of probability bins, n_k is the number of forecasts with the same probability, $\overline{o}_k$ presents the observed frequency, given forecasts of probability f_k, and $\overline{o}$ indicates the climatological probability of the event.

Skill scores are calculated with respect to a reference forecast as $\mathrm{BSS} = 1 - (\mathrm{BS}/\mathrm{BS}_{\mathrm{ref}})$. If a climatological forecast is taken as a reference, $\mathrm{BSS} = 1 - (\mathrm{BS}/b_{\mathrm{unc}})$, reliability of BSS $(\mathrm{B}_{\mathrm{rel}}) = 1 - (b_{\mathrm{rel}}/b_{\mathrm{unc}})$, and resolution of BSS $(\mathrm{B}_{\mathrm{res}}) = b_{\mathrm{res}}/b_{\mathrm{unc}}$.

3. STPM forecast results

3.1 *Temporally evolving predictor versus individual month predictor*

The first issue we address is which of the following strategies, a temporally evolving predictor and an individual month predictor, results in better forecast skill. Figure 4 shows the comparison of forecast skill between a temporally evolving predictor and an individual month predictor. The cross-validation was made for each of 31-yr (1979–2009) rainfall forecast experiments, each of which contained a 30-yr training period. We use the Taipei MAM rainfall forecast with predictor U925 as an example. Here the TCC between predicted and observed rainfall measures the forecast skill. In general, the temporally evolving U925 field maintains a high forecast skill (with a TCC value of 0.5–0.7), except for the 10-month lead case, which only contains preceding April information. The best forecast skill was achieved in the 7-month lead case when the U925 field from the preceding July to the preceding April was used. The forecast skills conducted by an individual month predictor, on the other hand, are not stable and vary in a great range, from −0.2 to 0.6. Among the individual month predictor cases, the predictions using the preceding February, June and May U925 fields show high skill, while the predictions using preceding December and August U925 fields show poor forecast results. A similar feature is found for other predictor fields (not shown). It suggests that the temporally varying predictors, in general, produce a higher and stable forecast skill than the individual month predictors.

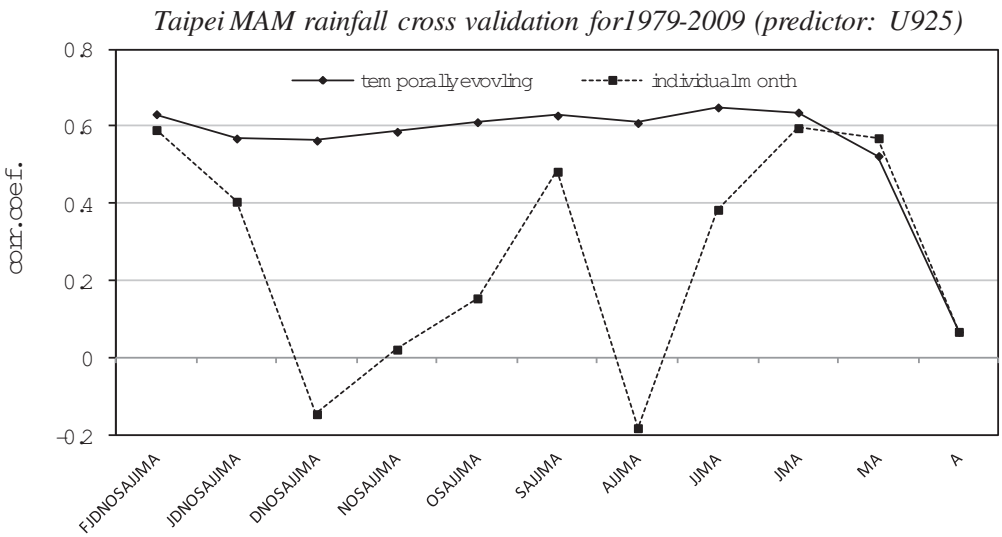

Fig. 4. STPM cross-validation skills measured by the TCC between predicted and observed MAM rainfall in Taipei for a temporally evolving predictor (solid line) and an individual month predictor (dash line). Here, the predictor is 925-hPa zonal wind field. Characters in *x*-axis indicate the preceding months used in the STPM. Characters shown at the dash line indicate the individual month used in the rainfall forecast.

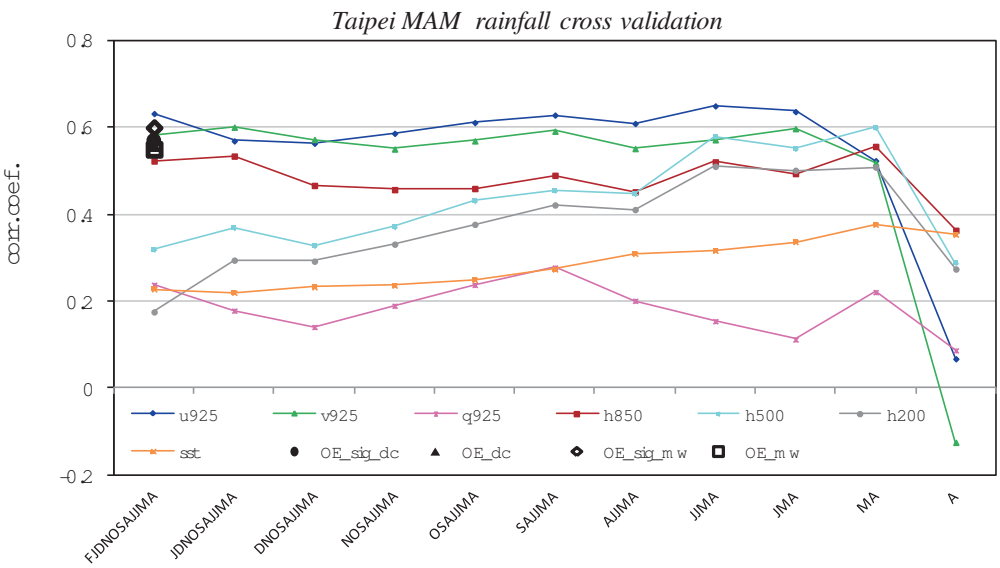

Fig. 5. STPM cross-validation skills of each predictor for the 0-month lead (i.e., FJDNOSAJJMA) up to 10-month lead (i.e., A) forecasts in Taipei. Temporally evolving predictors U925, V925, Q925, H850, H500, H200 and SST are represented by dark blue, green, pink, red, light blue, gray and orange curves, respectively. Skills of OE_sig (OE) based on double cross-validation and moving training window methods are represented by solid circle (triangle) and open diamond (square) respectively.

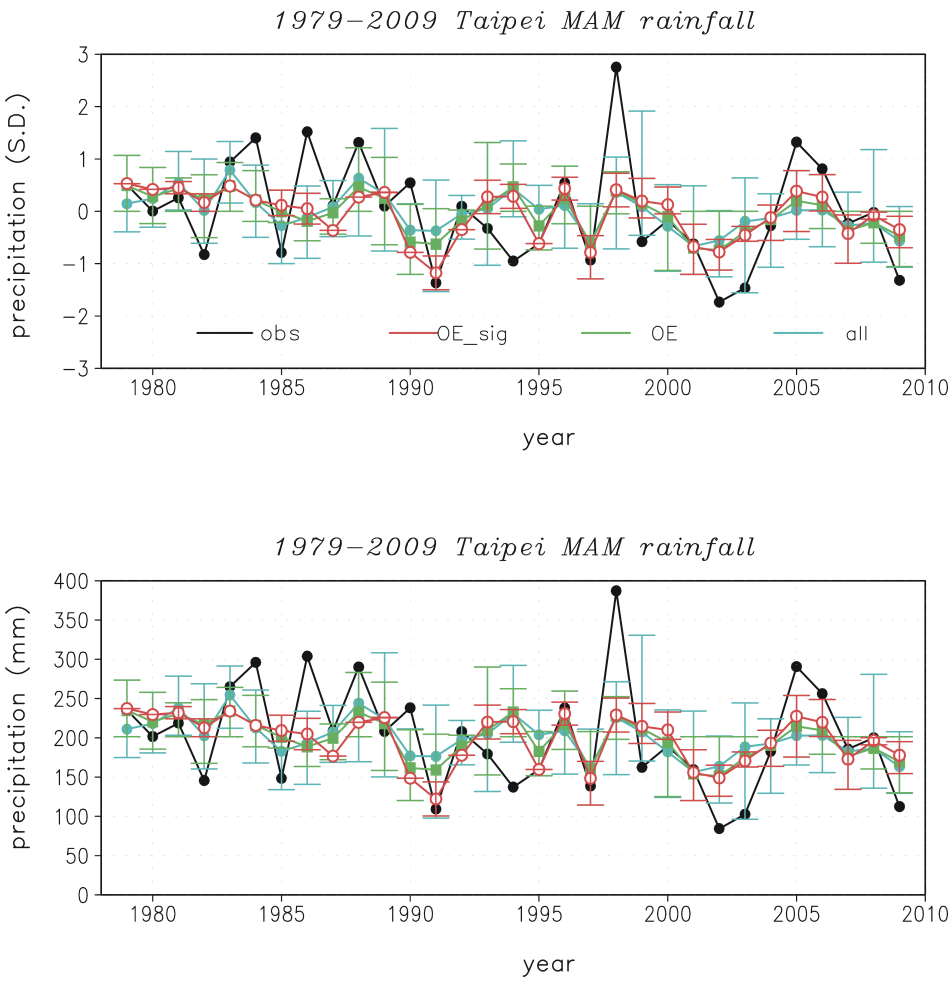

Fig. 6. (Upper) Time series of observed (black line) and predicted MAM rainfall anomalies (normalized by a standard deviation) in Taipei (red line: OE_sig, green line: OE, and blue line: SE) based on STPM forecasts. The error bars indicate the maximum and minimum of ensemble members. (Bottom) Same as upper panel except for the original rainfall values (unit: mm) without normalization.

Table 1. Original and corrected root-mean-square errors (unit: standard deviation) for OE_sig, OE and SE MAM rainfall forecast in Taipei. The corresponding amplifier coefficient for each ensemble method is also listed.

	Original RMSE	Corrected RMSE	Amplifier Coef.
OE_sig	0.83	0.83	1
OE	0.90	0.83	1.5
SE	0.95	0.84	1.5

Table 2. Brier Skill Score (BSS), reliability term of BSS (B_{rel}) and resolution term of BSS (B_{res}) for above-normal (AN), normal (N) and below-normal (BN) categorical MAM rainfall forecast in Taipei by using the STMP method. The probabilistic forecast skills based on the optimal ensemble (OE) and simple ensemble (SE) prediction are listed respectively.

	OE			SE		
	BSS	B_{rel}	B_{res}	BSS	B_{rel}	B_{res}
AN	0.37	0.89	0.19	0.36	0.64	0.47
N	0.29	0.77	0.36	0.10	0.50	0.20
BN	0.45	0.86	0.37	0.37	0.56	0.52

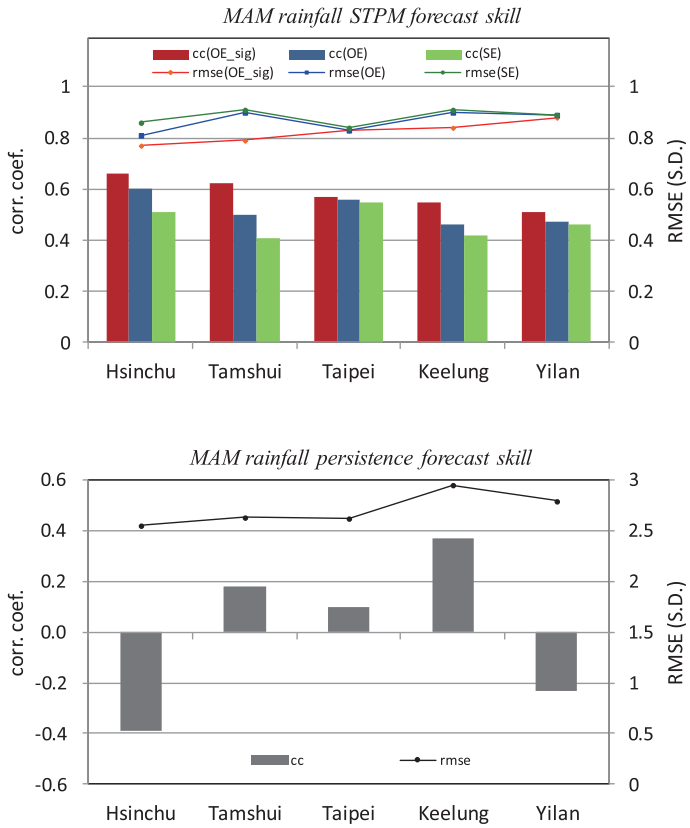

Fig. 7. Double cross-validation skills of MAM rainfall at five major stations in northern Taiwan based on (upper) STPM and (bottom) persistence forecasts. The bar denotes the TCC between observed and predicted rainfall. The curve denotes the root-mean-square error of predicted normalized rainfall (unit: standard deviation) after the amplifier coefficient is applied. Red, blue and green colors in upper panel indicate OE_sig, OE and SE, respectively.

3.2 *Effect of forecast lead time*

Figure 5 shows the Taipei MAM rainfall forecast skills of each predictor with different lead months. For example, February (January) and back to the preceding April predictor fields are used for the 0-month (1-month) lead forecast case. Only preceding April predictor field is used for the 10-month lead forecast. The result shows that U925 and V925 fields both have good skill (TCC$\sim$0.6) for 0-month to 9-month lead forecasts. Their forecast skills dramatically drop in the 10-month lead case, in which only the preceding April information is known. This implies that U925 and V925 are potentially excellent predictors for the spring rainfall forecast when their temporal evolutions are taken into account. Predictors, such as H850, are skillful at short lead time (0- and 1-month lead) forecast. For predictors H500, H200 and SST, the forecast skills increase as the lead month gets further away. Although the geopotential high fields show relatively low skill in Taipei as compared to 850-hPa wind fields, they serve as the best predictors in other stations. For instance, at Tamshui (Yilan and Keelung) stations, the 850-hPa (500-hPa and 200-hPa) geopotential high with 6–8 lead-month forecast cases have the highest skills (Figs not shown). Although the SST is not the best predictor for MAM rainfall forecast in northern Taiwan, its slow evolution feature and long memory have a remote impact on the atmospheric wind, humidity and pressure fields. The result suggests that the STPM has an advantage in long-lead climate forecast as long as statistically significant spatial-temporal variations in predictors are detected (Figs. 4, 5).

Among different lead time cases, we select the most skillful prediction of each large-scale predictor for optimal ensembles. Based on the 1979–2009 double cross-validated result, the optimal ensemble approaches perform well with TCCs of 0.57 and 0.56 for OE_sig and OE respectively (Fig. 5). Using a 20-year moving training period for the latest 11-year (1999–2009) independent forecast, similar to Kug et al. (2007), the TCCs of OE_sig and OE are 0.6 and 0.55 respectively (Fig. 5). It indicates that the optimal ensemble approach achieves better forecast skill for the Taipei station. The STPM forecast results at other stations will be shown in Subsection 3.5.

3.3 Improvement of rainfall root mean square error

The STPM forecasted MAM rainfall anomalies based on optimal and simple ensembles, along with the observed counterparts, are shown in Fig. 6. It appears that the interannual variations of the predicted anomalous rainfall in Taipei are generally smaller than the observation. In most years, the amplitude of predicted MAM rainfall is underestimated. The anomalous MAM rainfall in 1998 shows a large value of 3 standard deviations (∼400 mm) in observation, while it is about 1 standard deviation (∼250 mm) in the STPM. As a result, the RMSE of the forecasted rainfall field is quite large. Table 1 lists the RMSE values of the OE_sig, OE and SE predictions, respectively. The RMSEs based on the OE_sig prediction is 0.83, and it increases slightly in the OE and SE predictions.

To reduce the RMSE of the forecasted rainfall, an amplifier coefficient is introduced. Our strategy is to multiply the forecasted rainfall time series with a set of coefficients (e.g., 1, 1.5, 2, 2.5, 3, 3.5, and 4), and an optimal coefficient is determined based on the least square method. Applying the optimal coefficient to each of 31-year MAM rainfall predictions, we obtained an improved forecast with the RMSE reduced by 8–12% (see Table 1).

3.4 Probabilistic forecast results

The aforementioned skills are evaluated based on a deterministic forecast with use of either optimal or simple ensemble approach. The capability of STMP probabilistic forecast is further examined in this section. We consider a three-class categorical forecast of MAM precipitation. The category boundaries for terciles are at 33.3 and 66.7 percentiles to create below-normal (BN), normal (N) and above-normal (AN) categories.

For the AN categorical forecast of MAM rainfall in Taipei, both the OE and SE reveal high skill scores (BSS>0.36). Although the probabilistic prediction based on OE is more reliable than that of SE method, it has relatively poor resolution (Table 2). This low resolution is attributed to the small size of ensemble members for the probabilistic forecast at a single station. The results from the BN categorical forecast indicate that the STPM probabilistic prediction is highly skillful. The BSS reaches 0.37 for the SE forecast, and becomes 0.45 when the OE approach is applied. Similar to the AN case, the majority of the improvement of OE over SE comes from the reliability term (B_{rel}). For the normal categorical forecast, both the reliability and resolution are improved via the OE approach, leading to an increase of BSS (Table 2).

Table 3. Skills of below-normal (BN) categorical forecast of MAM rainfall at five major stations in northern Taiwan.

BN forecast	BSS	B_{rel}	B_{res}
Hsinchu	0.42	0.81	0.38
Tamshui	0.23	0.61	0.31
Taipei	0.45	0.86	0.37
Keelung	0.33	0.68	0.32
Yilan	0.40	0.73	0.48

In summary, the STPM is skillful, not only for deterministic forecast, but also for the probabilistic prediction of Taipei MAM rainfall. The OE method increases the probabilistic forecast skill by improving the reliability term in all three categories.

3.5 MAM seasonal rainfall forecasts in northern Taiwan

The deterministic forecast skill of spring rainfall at five major stations in northern Taiwan are shown in Fig. 7. Persistent forecast was also performed as a benchmark for comparison. Overall, the MAM rainfall forecasts based on the STPM are skillful in all five stations (upper panel of Fig. 7). The TCC and RMSE are both significantly superior to the persistent forecast, which reveals low (even negative) TCCs and very large RMSEs (bottom of Fig. 7). In the OE_sig forecast, the highest TCC skills appear in Hsinchu and Tamshui, where the forecast errors (RMSE) are smallest. The correlations in both the stations exceed 0.6, and the RMSE values are about 0.8. Although Yilan attains the lowest skill among the five stations in northern Taiwan, its TCC of the OE still reaches 0.5, which is significant at the 99% confidence level. The OE_sig approach increases the forecast skills significantly in all stations. The OE results are better than the SE results in terms of TCC, while showing a small improvement for RMSE

Table 4. List of best predictors and corresponding amplifier coefficient for each station. The number in bracket denotes the involved temporal information of predictor regarding to lead months. For example, "0" presents the predictor with 0-month lead information from February back to preceding April (e.g., FJDNOSAJJMA) while "1" denotes predictor with 1-month lead information from January back to preceding April (e.g., JDNOSAJJMA). "10" indicates the 10-month lead prediction in which only the preceding April information is involved.

Station	Predictors (number of lead months)	Amplifier coefficient
Hsinchu	U925(**1**), V925(**0**), Q925(**0**), H850(**8**), H500(**1**), H200(**1**), SST(**10**)	1.5
Tamshui	U925(**7**), V925(**7**), Q925(**9**), H850(**7**), H500(**7**), H200(**5**), SST(**10**)	1
Taipei	U925(**7**), V925(**0**), Q925(**10**), H850(**9**), H500(**10**), H200(**10**), SST(**9**)	1.5
Keelung	U925(**7**), V925(**9**), Q925(**9**), H850(**7**), H500(**7**), H200(**5**), SST(**7**)	1
Yilan	U925(**10**), V925(**9**), Q925(**0**), H850(**10**), H500(**10**), H200(**0**), SST(**10**)	1.5

as compared to the SE. It is noted that among five stations, the OE forecast in Taipei station is the closest to the SE forecast. This implies that seven predictors with different leads are all quite skillful for rainfall forecasts in Taipei. In this case the effect of setting significance criteria on ensemble forecast is relatively small.

Because spring drought is a serious concern in Taiwan, we focus on the skill of below-normal categorical prediction based on OE (Table 3). The probabilistic forecast results show that the STPM has high skill at all 5 stations. Among these stations, Taipei has the best BSS (0.45) while Tamshui has the lowest score (0.23). This below-normal categorical forecast is reliable with an averaged B_{rel} of 0.74.

4. Summary

A statistical model based on a spatial-temporal coupled pattern projection method (STPM) is developed to predict the MAM seasonal rainfall anomaly in northern Taiwan. The key feature of the STPM is to consider temporally varying large-scale fields in the preceding 11 months. Seven large-scale fields (including 925-hPa zonal and meridional wind, 925-hPa moisture, 850-, 500- and 200-hPa geopotential height, and SST) are used as predictors in the STPM. Because lag-correlation patterns between the spring rainfall in Taiwan and antecedent large-scale predictor fields are both space and time dependent, we only select domains where the correlation between the predictor and rainfall is statistically significant at the 95% confidence level. The cross-validation of hindcast results for the period of 1979–2009 shows that a temporally evolving predictor results in a higher, more stable forecast skill than that made by an individual month predictor. For each predictor, the best prediction is selected among different preceding months. An optimal ensemble (OE) strategy is further developed based on the performance of seven best prediction models derived from each of seven predictors. The OE method produces a skillful prediction because it excludes predictors with relatively poor skill. To improve the underestimated rainfall amplitude, an amplifier coefficient is introduced. The application of the amplifier coefficient leads to reduction of the rainfall RSME by 8–12%.

The double cross-validation result indicates that the STPM is skillful (with an averaged temporal correlation coefficient of about 0.6) in forecasting the MAM seasonal rainfall anomaly in northern Taiwan. Hsinchu shows the best forecast skill among five major stations in northern Taiwan, with the largest TCC of 0.66 and the smallest RMSE of 0.77. The spring rainfall forecast in Yilan is the least skillful, with a TCC of 0.51 and a RMSE of 0.88. In the double cross-validation procedure, the optimal predictors for OE prediction change each year. We counted the frequency of individual models for OE forecast over a 31-year (1979–2009) period. Table 4 lists the most skillful predictors which have the highest frequency for the OE and the corresponding amplifier coefficients at these five stations.

The STPM is not only skillful for the deterministic forecast but also informative for probabilistic prediction. A high BSS was achieved for STPM below-normal rainfall forecast. Because the lack of spring rainfall poses a serious threat to Taiwan, this skillful probabilistic prediction provides important information for the decision makers involved in water source management.

Although the STPM shows encouraging forecast results, there is a room to further refine the methodology and improve the predicted rainfall amplitude. In addition, the statistically significant signals of each dynamic and thermodynamic field associated with MAM rainfall forecast appear in various geographical locations and change with lead time (Fig. 2). The most skillful predictors are also station dependent (Table 4). These results

suggest that the variations of spring rainfall in northern Taiwan are modulated by complicated processes. The physical connection between the large-scale fields and the spring rainfall in northern Taiwan needs to be further explored. Given that CWB is currently developing a dynamical seasonal forecasting system, an alternative way is to build a dynamical-statistical rainfall forecast model based on the seasonal prediction system output.

Acknowledgements

The authors appreciate constructive comments from three anonymous reviewers. This work was supported by CWB phase-5 climate project, APEC Climate Center (APCC) international research project, and by the International Pacific Research Center (IPRC) that is sponsored by the Japan Agency for Marine-Earth Science and Technology (JAMSTEC), NASA (NNX07AG53G) and NOAA (NA17RJ1230). This is SOEST contribution number 8562 and IPRC contribution number 856.

References

Chang, C. P., Y. S. Zhang, and T. Li, 2000: Interannual and interdecadal variations of the East Asian summer monsoon and tropical Pacific SSTs. Part I: Roles of the subtropical ridge. *J. Climate*, **13**, 4310–4325.

Chen, C.-S., and Y.-L. Chen, 2003: The rainfall characteristics of Taiwan. *Mon. Wea. Rev.*, **131**, 1323–1341.

Chen, G. T. J., Z. H. Jiang, and M. C. Wu, 2003: Spring heavy rain events in Taiwan during warm episodes and the associated large-scale conditions. *Mon. Wea. Rev.*, **131**, 1173–1188.

Chen, J.-M., T. Li, and J. Shih, 2008: Asymmetry of the El Niño-spring rainfall relationship in Taiwan. *J. Meteor. Soc. Japan*, **86**, 297–312.

Feddersen, H., A. Navarra, and M. N. Ward, 1999: Reduction of model systematic error by statistical correction for dynamical seasonal prediction. *J. Climate*, **12**, 1974–1989.

Gong, D.-Y., and C.-H. Ho, 2003: Arctic oscillation signals in the East Asian summer monsoon. *J. Geophys. Res.*, **108**, 4066, doi:10.1029/2002JD002193.

Hung, C.-W., H.-H. Hsu, and M.-M. Lu, 2004: Decadal oscillation of spring rain in northern Taiwan. *Geophys. Res. Lett.*, **31**, L22206, doi:10.1029/2004GL021344.

Jiang, Z., G. T.-J. Chen, and M.-C. Wu, 2003: Large-scale circulation patterns associated with heavy spring rain events over Taiwan in strong ENSO and non-ENSO years, *Mon. Wea. Rev.*, **131**, 1769–1782.

Kalnay, E., and Coauthors, 1996: The NCEP/NCAR 40-Year Reanalysis Project. *Bull. Amer. Meteor. Soc.*, **77**, 437–471.

Kug J.-S., J.-Y. Lee, and I.-S. Kang, 2007: Global Sea Surface Temperature Prediction Using a Multi-model Ensemble. *Mon. Wea. Rev.*, **135**, 3239–3247.

Kug, J.-S., J.-Y. Lee, I.-S. Kang, B. Wang, and C. K. Park, 2008: Optimal multimodel ensemble method in seasonal climate prediction. *Asia-Pacific J. Atmos. Sci.*, **44**, 233–247.

Lu, R., 2001: Interannual variability of the summertime North Pacific subtropical high and its relation to atmospheric convection over the warm pool. *J. Meteor. Soc. Japan*, **79**, 771–783.

Murphy, A. H., 1973: A new vector partition of the probability score. *J. Appl. Meteor.*, **12**, 595–600.

Smith, T. M., and R. W. Reynolds, 2004: Improved extended reconstruction of SST (1854–1997). *J. Climate*, **17**, 2466–2477.

Tao, S. Y., and L. X. Chen, 1987: A review of recent research of the East Asian summer monsoon in China. *Monsoon Meteorology*, C. P. Chang and T. N. Krishnamurti, Eds., Oxford University Press, 60–92.

Wang, B., R. Wu, and K.-M. Lau, 2001: Interannual variability of the Asian summer monsoon: Contrasts between the Indian and the western North Pacific–East Asian monsoon. *J. Climate*, **14**, 4073–4090.

Wang, B., and Q. Zhang, 2002: Pacific–East Asian teleconnection. Part II: How the Philippine Sea anomalous anticyclone is established during El Nino development. *J. Climate*, **15**, 3252–3265.

Watanabe, M., and F.-F. Jin, 2002: Role of Indian Ocean warming in the development of the Philippine Sea anticyclone during El Niño. *Geophys. Res. Lett*, **29**, doi: 10.1029/2001GL014318.

Wilks, D. S., 1995: *Statistical methods in the atmospheric sciences*. Academic Press, Dublin, 467 pp.

Wu, B., T. J. Zhou, and T. Li, 2009: Contrast of rainfall—SST relationships in the western North Pacific between the ENSO developing and decaying summers. *J. Climate*, **22**, 4398–4405.

Wu, B., T. Li, T. Zhou, 2010: Asymmetry of atmospheric circulation anomalies over the western North Pacific between El Niño and La Niña. *J. Climate*, **23**, 4807–4822.

Wu, R., and B. P. Kirtman, 2007: Observed relationship of spring and summer East Asian rainfall with winter and spring Eurasian snow. *J. Climate*, **20**, 1285–1304.

Yang, S., K.-M. Lau, S.-H. Yoo, J. L. Kinter, and C.-H. Ho, 2004: Upstream subtropical signals in preceding the Asian summer monsoon circulation. *J. Climate*, **17**, 4213–4229.

Yen, M. C., and T. C. Chen, 2000: Seasonal variation of the rainfall over Taiwan. *Intl. J. Climatol.*, **20**, 803–809.